Mon. Not. R. Astron. Soc. **000**, 000–000 (0000) Printed 12 April 2001 (MN LaTeX style file v1.4)

The jets in 3C 66B

M.J. Hardcastle, P. Alexander, G.G. Pooley and J.M. Riley
Mullard Radio Astronomy Observatory, Cavendish Laboratory, Madingley Road, Cambridge

Accepted 1995 August 4. Received 1995 August 3; in original form 1994 May 24

ABSTRACT
The nearby FRI radio source 3C 66B has been studied with the VLA at 1.5, 8 and 15 GHz with high resolution and sensitivity. The first detailed maps of the counterjet are presented. Polarization maps in the jet and counterjet are shown; in each a resolved parallel-field region surrounds a central core which changes from a parallel to a perpendicular field configuration. A model of the jets involving a relativistic central region and a slower outer sheath is discussed, and in this context 3C 66B is compared with similar sources.

Key words: galaxies: individual: 3C 66B – galaxies: jets – radio continuum: galaxies

1 INTRODUCTION

The radio galaxy 3C 66B is a nearby bright FRI source, identified with an ED2 galaxy at a redshift of 0.0215 (Matthews, Morgan & Schmidt 1964). The jet in 3C 66B is one of only a few which are visible in both the optical and radio wavebands, and was originally discovered by Northover (1973): the optical jet was first detected by Butcher, van Breugel & Miley (1980). Maccagni & Tarenghi (1981) found extended X-ray emission around the source, indicating densities sufficient to confine it. Leahy, Jägers & Pooley (1986, hereafter LJP) presented detailed radio observations of the source as a whole and of the jet with the VLA at 1.4, 1.6 and 5 GHz, with the Cambridge 5-km telescope at 2.7 GHz and with the Westerbork telescope at 608 MHz, 1.4 and 5 GHz. Fraix-Burnet et al. (1989a, 1989b) identified five knots in the optical structure of the jet with five similarly-placed knots in the radio maps of LJP, and detected polarization in them, providing convincing evidence that the optical emission is synchrotron in origin. Macchetto, Albrecht & Barbieri (1991) presented an *HST* Faint Object Camera image at 3100 Å (with a resolution of 0.1 arcsec), which showed for the first time filamentary structure in the jet: Jackson et al. (1993: JSMM) compared this with a high-resolution (0.25 arcsec) VLA map at 15 GHz. Here we present observations of the jet with the VLA at several resolutions and frequencies, which provide further information on the total intensity, spectral index and magnetic field structure of the jet and counterjet.

2 OBSERVATIONS

We observed 3C 66B at the L, X and U bands of the VLA, using two IFs of bandwidth 50 MHz at frequencies of 1.36 and 1.66 GHz, 8.01 and 8.41 GHz and 14.7 and 15.2 GHz respectively (except at C-array X band, for which IFs of 8.41 and 8.46 GHz were used). The data from the different IFs were concatenated and treated as a single database at an intermediate frequency — this procedure improves the coverage of the *u*-*v* plane, essential for mapping a complex object like 3C 66B, at the cost of a slight uncertainty in the flux measured from final maps because of spectral gradients between the two IFs. This uncertainty is below the level of the thermal noise for the 8 GHz dataset when maps from the single and combined frequencies are compared.

Observational details are summarized in table 1. The A-array data were obtained on 1991 August 19, the B-array data on 1991 November 5, and the C-array on 1994 Nov 10. (The B configuration was unusual, in that the most distant antenna on the eastern arm of the VLA was in the position appropriate for A rather than B configuration, but this does not seem to have affected the quality of the data.) The flux density calibrators were 3C286 and 3C48. Since no suitable polarization position angle calibrator was observed in B configuration, the position angles were deduced by comparison with the A-configuration data at both frequencies; in the other configurations 3C286 was used as the position angle calibrator. The data were reduced using the NRAO AIPS package in the standard manner. The datasets from the different configurations were reduced separately by several iterations of CLEANing and phase self-calibration, together with low-level data editing to eliminate bad baselines. After correction for radio nucleus variability (see section 3.1) the lower-resolution datasets were self-calibrated using a good CLEAN component model from the higher-resolution ones (to ensure phase compatibility) and were then merged with them with no reweighting. Further CLEANing and self-calibration were then used on the merged dataset to produce the final images.

3C 66B is a large source (several arcminutes in largest angular size) and the data we have on it does not sample the *u*-*v* plane sufficiently to map it with complete accuracy. The missing short baselines manifest themselves as a negative 'bowl' on either side of the jet, corresponding to the deconvolution algorithm's lack of information about large angular scales. The VLA is insensitive to structure with angular scale above 60 arcsec for 8-GHz C-array observation, 38 arcsec for 1.4-GHz A-array, and 12 arcsec for 15-GHz B-array. All structures in the maps are affected by this undersampling, but large areas of smooth emission are particularly vulnera-

Table 1. Observations of 3C 66B with the VLA

Configuration	Time		
	L-band	X-band	U-band
A	0.5 h	2.0 h	5.0 h
B		2.5 h	2.5 h
C		1.0 h	

ble; it is important to bear this in mind when comparing maps at different frequencies.

Bandwidth smearing is significant at the 5 per cent level at 28 synthesised beamwidths from the pointing centre at 1.4 GHz, limiting the accuracy of the maps at this frequency at distances of 30 arcsec or more from the radio nucleus. The errors caused by inadequate deconvolution (and subsequent poor self-calibration) of the bright bandwidth-smeared source 3C66A are the dominant ones in this dataset.

In addition to our new VLA observations, total intensity and polarization maps from the observations of LJP at 1.25-arcsec resolution (1.4, 1.6 and 5 GHz) and 0.35-arcsec resolution (5 GHz) were available to us. We made some observations of 3C 66B with the Cambridge Ryle telescope to determine the flux density of the radio nucleus at 15 GHz.

3 RESULTS

We use $H_0 = 50 \text{ km s}^{-1} \text{ Mpc}^{-1}$, $q_0 = 0.5$, for which 1 arcsec is equivalent to a projected distance of 600 pc. Spectral index is defined in the sense $S \propto \nu^{-\alpha}$. All maps are made with circular Gaussian restoring beams and the resolution quoted is the full width at half maximum of the Gaussian.

The relative scales of the different maps are shown in Fig. 1. For ease of identification and comparison between maps, the features in the figures are labelled with a modified version of the notation of Fraix-Burnet et al. (1989a). Bright knots are labelled with capital letters (A – F). The optical jet of Macchetto et al. (1991) extends approximately to knot E.

3.1 The radio nucleus

The radio nucleus is variable on timescales of months. Table 2 summarizes the data available on the flux densities at different frequencies, generally estimated by integration of a small region around the nucleus (except in the case of the Ryle telescope observations, where the fluxes were estimated directly from appropriate baselines). Errors are due to the small uncertainty in primary flux calibration and the difficulty in ensuring that none of the surrounding diffuse structure is included in the integration.

3.2 Structure at high resolution

Fig. 2 shows a linear greyscale of the 8-GHz map at 0.25-arcsec resolution. The r.m.s. off-source noise is 25 μJy. The 15-GHz dataset at similar resolution shows the same features but with less sensitivity; at the full resolution of the VLA at this frequency (0.15 arcsec) the noise is so high that only the radio nucleus can be detected above it. 15-GHz maps are therefore not presented.

The overall structure in our maps at this resolution agrees very well with that in the 15-GHz map of JSMM and the *HST* image of Macchetto et al. (1991). (The barring perpendicular to the jet visible on our 8-GHz image is an artefact which we believe to be due to the bright and variable nucleus.)

There are three small knots at the base of the jet, the first (knot A) at 0.9 arcsec from the nucleus (a projected distance of 550 pc) and the last at 1.8 arcsec (1.1 kpc). The jet becomes much brighter at knot B and reaches its brightest at about 2.9 arcsec (1.7 kpc) from the nucleus; at the same time its opening angle clearly increases. The shape of the region B is particularly interesting: the knot is at a distinct angle to both the entering and the leaving jets. The knots C, D and E are all visible on the *HST* image.

The images provide some evidence for the double filamentary structure claimed by Macchetto et al. in the optical and by JSMM at 15 GHz. However, as can be seen in the contour map (Fig. 3), even the clearest region where a double-stranded structure might be plausible (between knots C and D) involves brightness contrasts at only around the 3-4σ level. Much of the structure described in detail by JSMM is not consistent between their maps and ours. An image with still higher resolution and sensitivity is needed before a detailed analysis of the filamentary structure is warranted.

At this resolution and sensitivity the counterjet is almost invisible and no maps of it are shown.

3.3 Structure at intermediate resolution

Fig. 4 shows an 8-GHz map of the jet and counterjet at 1.25-arcsec resolution (chosen to be comparable with the highest resolution available at L-band, as used in LJP): the brightest knots are labelled for comparison with the high-resolution images. The apparent lumpiness of the distant parts of the source is due partly to lack of sensitivity and partly to comparative under-sampling of the *u-v* plane at these structure scales. Low-surface-brightness extensions to the east and west are not shown.

This maps shows for the first time structures in the fainter parts of the source. Particularly notable on the jet side are the quasi-periodic variations in the direction of the ridge line of the jet, starting on a small scale near knot E at about 10 arcsec (6 kpc) from the nucleus and increasing in amplitude for a further 25 arcsec before disappearing into the noise. These are visible at all frequencies.

The opening angles of the jet and counterjet appear more or less constant, although there is a point about 40 arcsec from the nucleus at which the jet appears to stay constant in width for a while. This is consistent with the results of LJP.

Detailed structure in the counterjet is seen for the first time in the 8 GHz images (see Fig. 5). The counterjet appears much more diffuse than the jet, and is not so consistently centre-brightened.

3.4 Asymmetries

The observations in the preceding two sections show a high degree of asymmetry between the jet and counterjet. For as far as the counterjet can be observed the jet is consistently brighter, although the ratio of the surface brightnesses of the jet and counterjet at comparable distances from the nucleus decreases towards unity more or less monotonically over that range. On larger scales, the low-resolution Westerbork telescope maps of LJP show two lobes of very similar size and surface brightness. On smaller scales, Giovannini et al. (1993) report unpublished VLBI observations by Bartel showing a one-sided parsec-scale jet in 3C 66B in the same position angle as the bright kiloparsec-scale jet. These observations seem to confirm the trend seen in our results for the jet-counterjet asymmetry to decrease with distance from the nucleus. Results such as

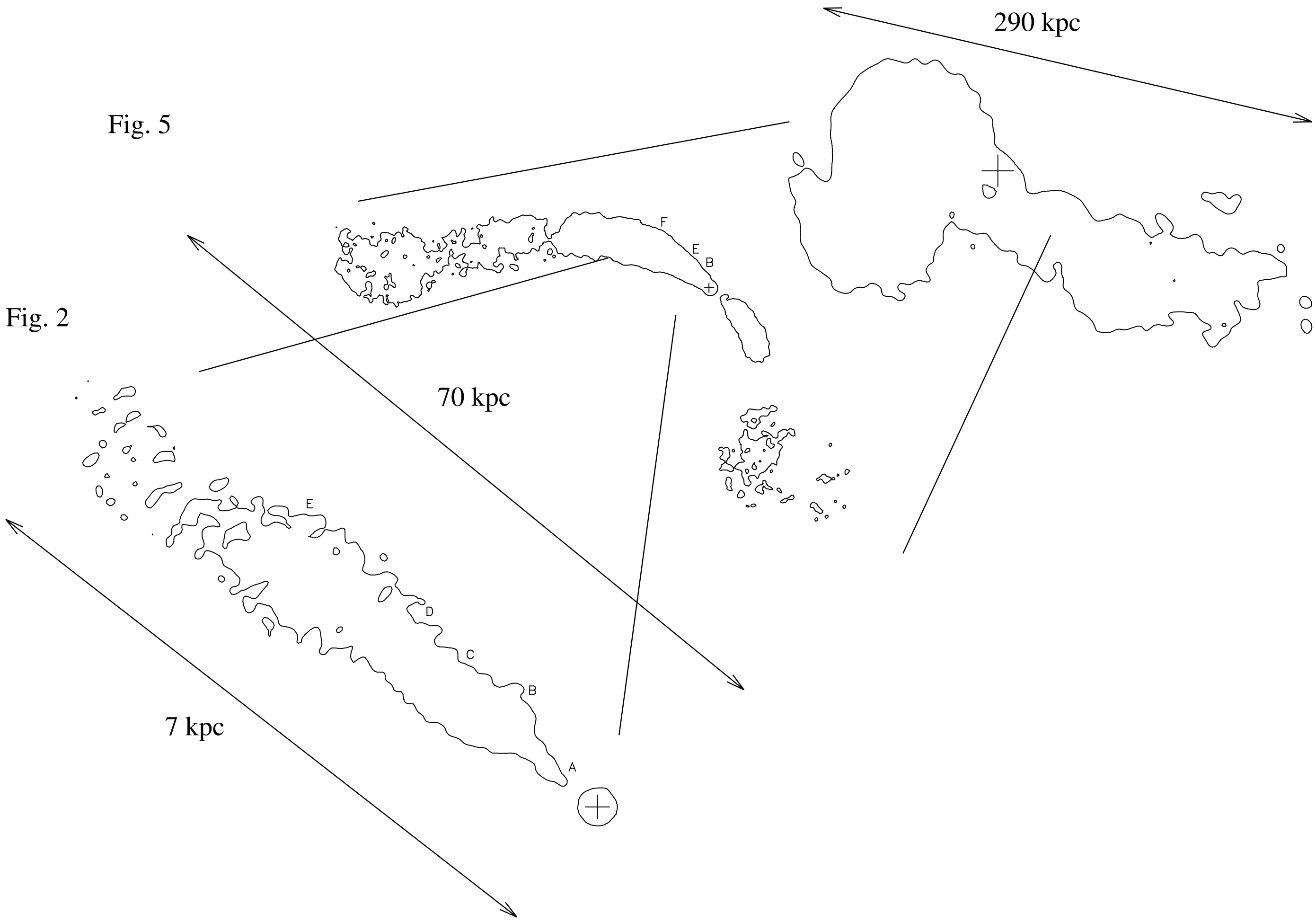

Figure 1. Relative scales of the different maps shown. The map in the top right shows the 4 mJy beam^{-1} contour of a 1.5 GHz VLA C-array image with 12.5 arcsec resolution. The maps in the centre and left show 2 mJy beam^{-1} contours of 8-GHz images at 1.25 and 0.25 arcsec resolution respectively. Crosses mark the approximate position of the radio nucleus.

Table 2. Flux densities from the radio nucleus

	$S_{1.4}$/mJy	$S_{1.6}$/mJy	S_5/mJy	$S_{8.4}$/mJy	S_{15}/mJy
1972 Jul[1]			240 ± 40		
1982 May[2]	188 ± 9	167 ± 10	182 ± 6		
1982 Sep[2]			256 ± 9		
1991 Jul[3]					207
1991 Aug[4]	178 ± 10	187 ± 10		223 ± 11	207 ± 10
1991 Nov[4]				191 ± 10	165 ± 8
1992 Jan[3]					172
1992 Nov[5]					175 ± 12
1994 Apr[5]					210 ± 15
1994 Nov[4]				238 ± 10	
1995 Mar[4]				213 ± 15	
1995 Apr[5]					202 ± 10

[1] Northover (1973). [2] LJP. [3] JSMM. [4] Our VLA observations. [5] Our Ryle telescope observations.

these are often interpreted as evidence for relativistic velocities in the inner parts of the jets, a question which will be discussed in Section 4.1.

3.5 Polarization structure

Polarization maps use points above 3σ in both the total and polarized intensity maps and show 'magnetic field angle', determined by assuming a constant rotation measure of -90 rad m^{-2} across the source (following LJP: the errors caused by this assumption are of the order of a few degrees at the frequencies concerned).

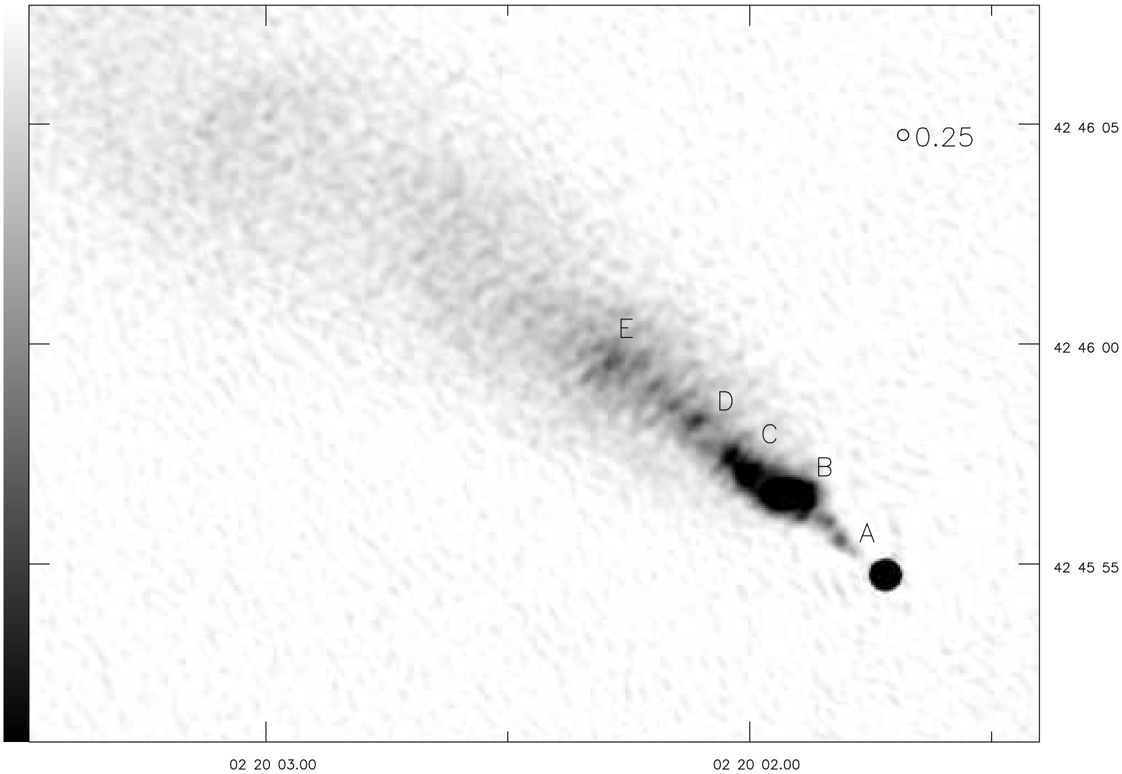

Figure 2. Greyscale of the 8-GHz map at 0.25-arcsec resolution; black is 1 mJy beam^{-1}

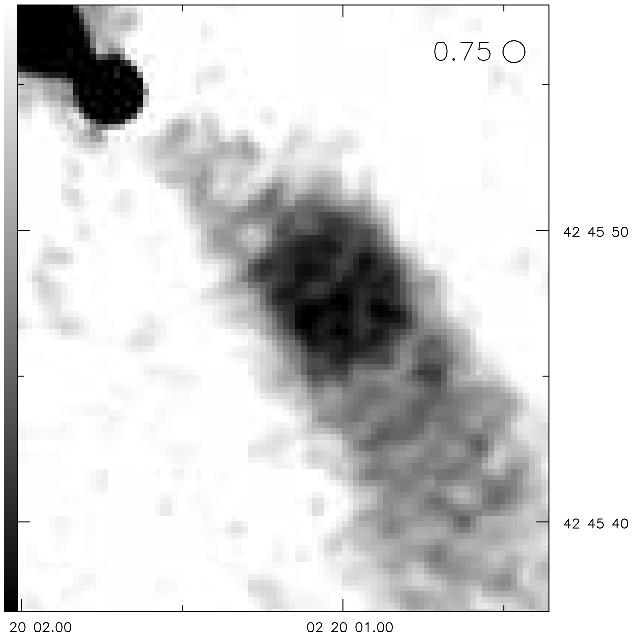

Figure 5. 8-GHz map of counterjet at 0.75-arcsec resolution; black is 4 mJy/beam

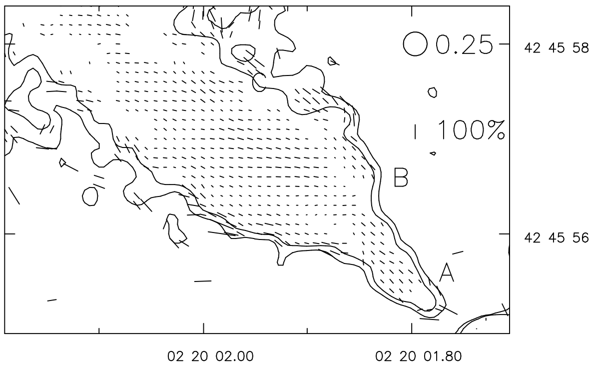

Figure 7. Detail of 8-GHz polarization map at 0.25-arcsec resolution. Contours at 0.1, 0.2 mJy beam^{-1}

Fig. 6 shows maps of degree of polarization and magnetic field angle at 8 GHz and 1.25 arcsec resolution. (Maps at other frequencies are similar but noisier and are not shown.) The nucleus itself appears to be polarized at the 0.5 per cent level. The jet and counterjet are quite highly polarized (between 10 and 40 per cent in the main part of the jet, and 20 – 50 per cent in the counterjet) implying well-ordered magnetic fields on kpc scales. On the jet side the magnetic field is parallel to the jet for the first 1.2 pc (2 arcsec), best seen in the high resolution polarization map (Fig. 7): in the bright knots B and C there are regions where it is at an angle of about 30° to the jet direction (more or less aligned with the direction of

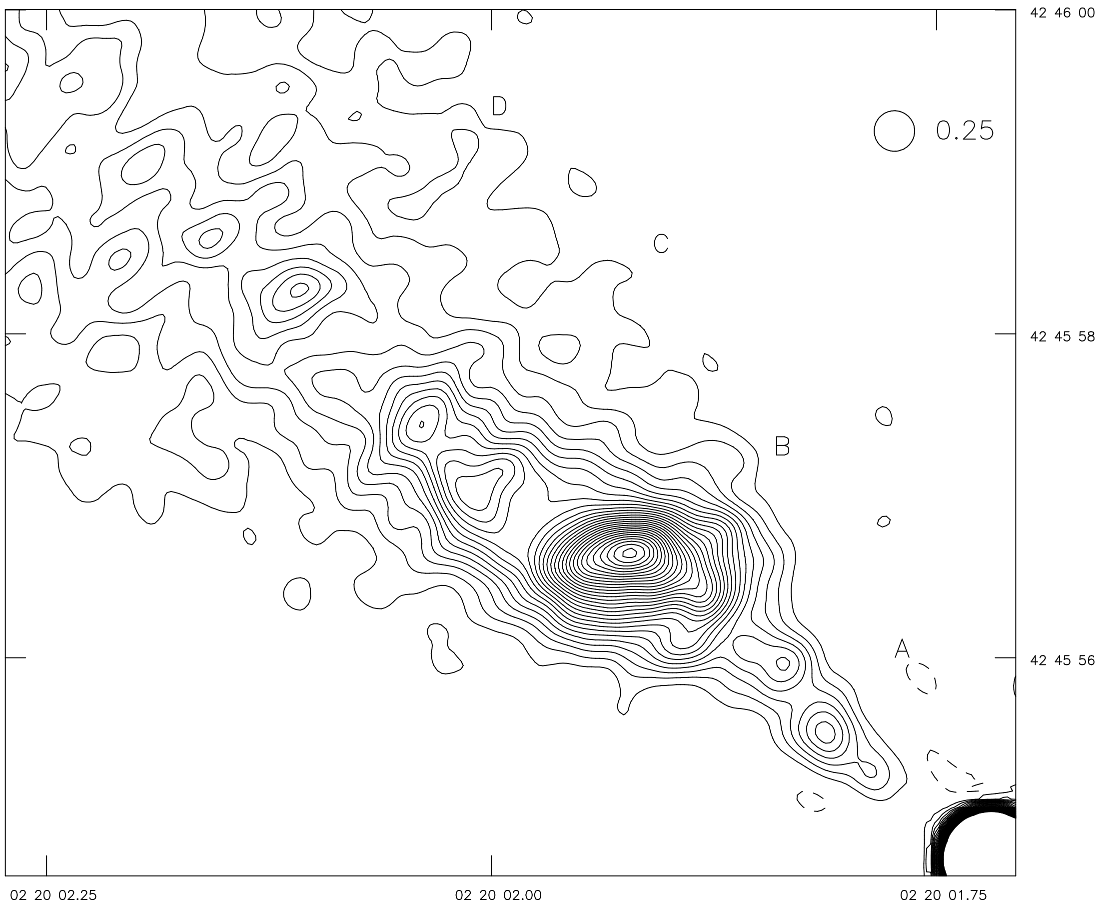

Figure 3. 8-GHz map at 0.25-arcsec resolution. Contours at $-0.1, 0.1, 0.2, 0.3 \ldots 4$ mJy beam^{-1}. Negative contours are dashed.

elongation of the knot B) and by knot E (8 arcsec from the nucleus) the B-field in the centre of the jet is perpendicular. Fig. 8 shows the variation of degree of polarization as a function of distance along the jet, taken along the ridge line; the change in polarization angle takes place in the region of depolarization between 6 and 10 arcsec (a projected distance of ~ 2.5 kpc).

At the edges of the jet the field remains parallel, with a higher degree of polarization (typically 30 per cent, as opposed to around 10 per cent in the jet centre). There is a clear region of depolarization between the parallel and perpendicular field alignments. A remarkable circular field structure can be seen centred at 18 arcsec from the nucleus, coincident with the large bright region F and presumably related to the change in jet direction that begins at about this point. Further out from the nucleus the field in the jet centre follows the wiggles in the jet closely, remaining more or less perpendicular to the jet axis in spite of its changes in direction. There are some indications that the parallel-field sheath is still present at 30 arcsec or more away from the nucleus.

The counterjet is unpolarized above the 3σ limit close to the nucleus. Further out, between 6 arcsec and about 15 arcsec, there is a clearly delineated central region with perpendicular B-field surrounded by a sheath with B-field parallel. The sheath in the counterjet appears to be about 1.3 arcsec (800 pc) thick, as opposed to that in the jet which is typically 0.8 arcsec (500 pc) across (just resolved in our 0.75-arcsec resolution maps). The lower limits placed

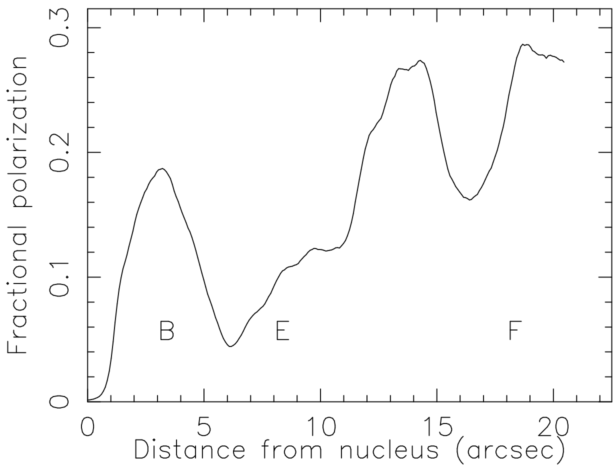

Figure 8. Variation of fractional polarization with distance along the jet

on the sheath thickness by LJP were due to the lower sensitivity of their observations.

Further still from the nucleus, our polarization data are in good agreement with those of LJP, showing the highly polarized terminations of the jets.

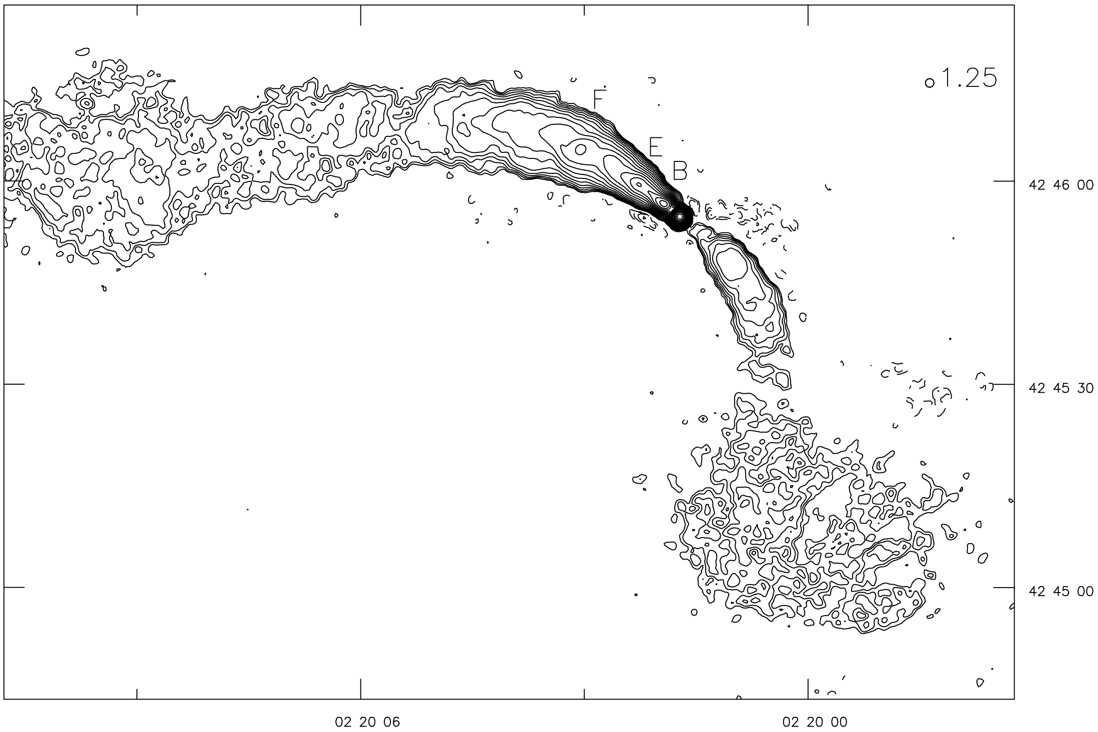

Figure 4. 8-GHz map at 1.25-arcsec resolution. Contours at $0.1 \times (-1, 1, \sqrt{2}, 2, 2\sqrt{2}, \ldots)$ mJy beam^{-1}. Negative contours are dashed. Peak 180 mJy beam^{-1}; r.m.s. off-source noise 25 μJy.

3.6 Spectral indices

At 0.25-arcsec resolution we find that the spectral indices between 8 and 15 GHz of the bright knots B–E and the regions between them are very similar (between 0.5 and 0.6). These results are consistent with the high-resolution radio-optical spectral index maps of JSMM, which show a constant spectral index of 0.8 – 0.85 in the region within 5 kpc (8 arcsec) of the nucleus over the central 1 kpc of the jet.

On larger scales, the data are affected by the undersampling problem discussed in section 2; the best we can say, having made maps at 1.5 and 8.4 GHz with matched longest and shortest baselines, is that there is no evidence for significant change in the spectral index between these two frequencies out to knot F (20 arcsec from the nucleus). The typical spectral index is 0.5 ± 0.05 over this region. There is insufficient sensitivity at any frequency other than 8 GHz to measure spectral index in the counterjet reliably. In the few pixels where a good value can be measured it is typically 0.7 ± 0.1, steeper than that in the jet.

These results are in agreement with the lower-frequency measurements of LJP.

3.7 Depolarization and rotation measure

Our data largely confirm the rotation measure map of LJP at 1.25-arcsec resolution, without providing any additional information: a map is therefore not shown.

Unfortunately our signal-to-noise ratio in the counterjet is not sufficient at 1.4 GHz to allow us to compare depolarization in the jet and counterjet, although this result would be very important in constraining orientation and Doppler beaming models (see below). The results of LJP are very marginal on the counterjet side because of their low resolution and sensitivity, but might be interpreted as showing greater depolarization there. On the jet side, there is clear depolarization between 1.4 and 8 GHz, with the depolarization measure DP (defined as the ratio of the fractional polarization at the lower frequency to that at the higher frequency: low values of DP imply strong depolarization) being typically about 0.7.

4 DISCUSSION

4.1 Velocities in the jets

We have shown (Section 3.4) that there is a high degree of asymmetry in surface brightness between the jet and counterjet of 3C 66B at distances up to a few kiloparsecs from the radio nucleus, and that the source becomes very symmetrical in terms of lobe structure and surface brightness on the largest scales. The flat-spectrum radio nucleus of the source is highly variable (up to 35 per cent at high frequencies on a timescale of months: Section 3.1). The model most commonly proposed to explain this type of object is one in which the jets near the nucleus are relativistic and their emission is Doppler beamed toward or away from the observer: as the jets decelerate the flux asymmetry decreases. In this section we show that the data on 3C 66B are adequately explained by this model, although a model in which the jet in 3C 66B is currently intrinsically brighter than the counterjet is not ruled out by our observations.

The jet in 3C 66B is brighter than the counterjet as far as they can both be traced; the counterjet disappears into a 'bubble' of diffuse emission after about 25 arcsec. We can apply the relativistic beaming model to 3C 66B on the hypothesis that the jets are of

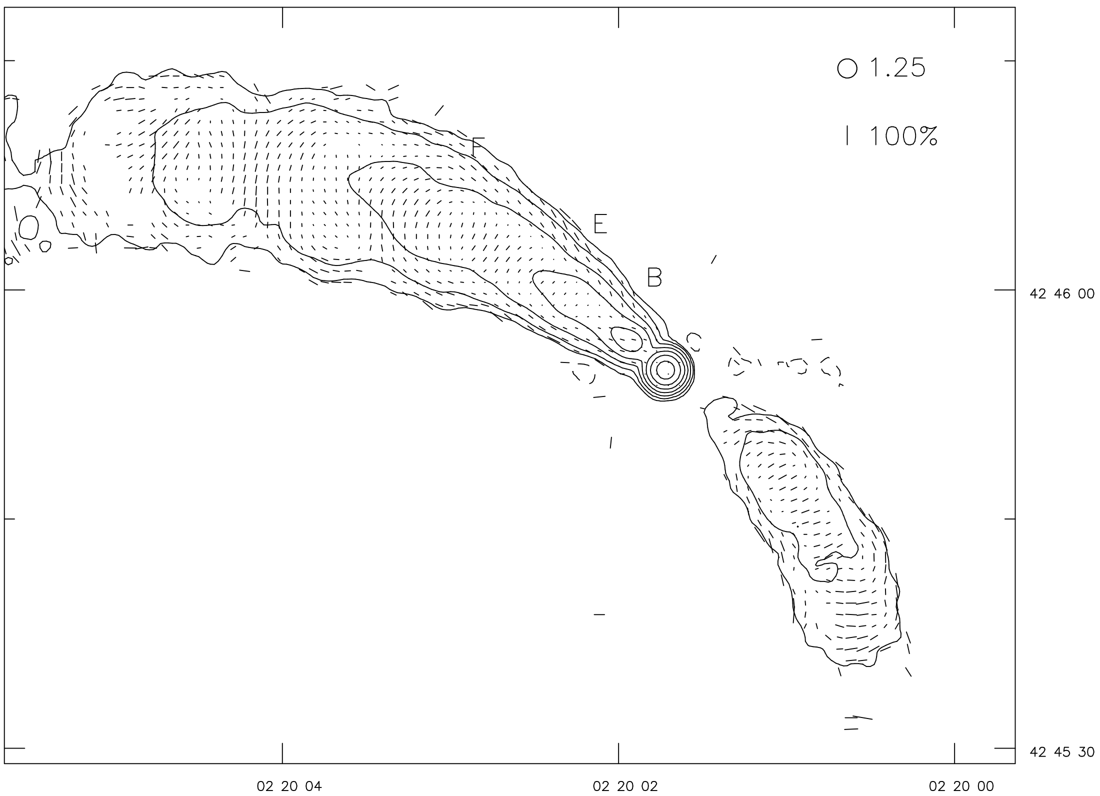

Figure 6. 8-GHz polarization map at 1.25-arcsec resolution. Contours at $0.2 \times (1, 2\sqrt{2}, 8, \ldots)$ mJy beam^{-1}

equal intrinsic power, a reasonable assumption given the similarity of the energies of the two lobes on the large scale. However, there are several complications. Both jets are curved, and the angles made by the bulk flow with the line of sight therefore change with distance away from the nucleus. In general, the angles made with the line of sight in the jet and counterjet may be quite different, although they are likely to be similar close to the nucleus.

If we apply a naïve model in which all the flux asymmetry is due to relativistic beaming, all jet material moves at the same bulk velocity βc and the jet and counterjet make a single angle θ to the line of sight, we may use the standard formula

$$R = \left(\frac{1+\beta\cos\theta}{1-\beta\cos\theta}\right)^{2+\alpha}$$

(where R is the flux ratio between jet and counterjet) and the integrated flux ratios of the jet and counterjet at different angular distances to find $\beta\cos\theta$ as a function of distance from the nucleus. This is plotted in Fig. 9. It can be seen that $\beta\cos\theta$ initially falls with distance from the nucleus, as would be expected for a decelerating jet with constant θ. Supposing the model to be more or less accurate for the inner few kiloparsecs of the jet (which is reasonable, since the jet appears straight in the high-resolution maps of Fig. 2) values of $\beta\cos\theta$ around 0.6 constrain the angle to the line of sight of the emerging jet to be $\theta \lesssim 53°$. Further from the nucleus $\beta\cos\theta$ begins to rise again, corresponding to the disappearance of the counterjet here. This is not consistent with a simple model, but it is clear from our maps that the jets bend and that the assumption of constant θ, at least, must be wrong on these scales.

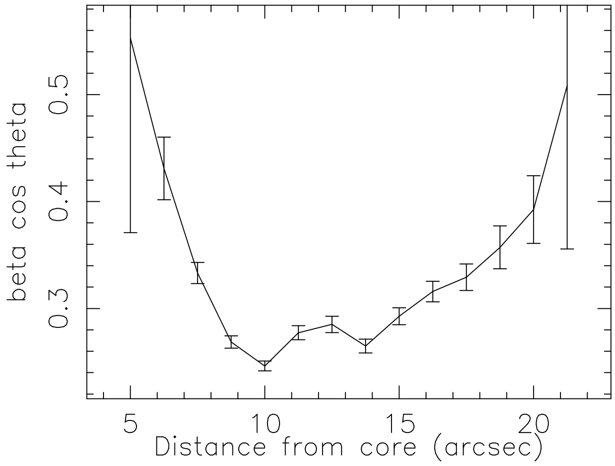

Figure 9. $\beta\cos\theta$ against distance from the nucleus

It is well known (Burch 1979) that the brightness decline in the jets of FRIs is sub-adiabatic; that is, their surface brightness drops with distance along the jet much less rapidly than would be expected for a smooth uniformly expanding jet with no particle reacceleration. The most persuasive way to overcome this problem comes from the semi-empirical model by Bicknell and others (e.g. Bicknell 1986) in which the jets are turbulent and entrain external material as they decelerate; this both removes the assumption of constant velocity and allows particle reacceleration (discussed below in section 4.5). A fit of Bicknell's model to a sample of low-luminosity sources (Bicknell et al. 1990) has suggested jet velocities in the range 10^3 – 10^4 km s^{-1}. It may be more plausible on theoretical grounds (Komissarov 1993) that only a boundary layer of the jet should be turbulent, but it is not easy observationally to separate the limb-brightening effects this would produce from those which could be an effect of differential relativistic beaming. It has been thought to be difficult (e.g. Parma et al. 1993) to reconcile the two different velocity régimes required by the turbulent jet and relativistic beaming models: in the case of 3C 66B, deceleration by factors of between 10 and 100 over the inner few kiloparsecs would be required to allow both models to describe the source successfully. However, Bicknell (1994) has analyzed the dynamics of a relativistic entraining jet in some detail; he shows that the velocity at which a relativistic jet has decelerated to a transonic Mach number (presumed to be the region at which large-scale turbulent entrainment begins) must lie between about 0.3–$0.7c$ (values consistent with our constraints on $\beta \cos\theta$) and that significant deceleration on the kiloparsec scale thereafter is dynamically feasible. A full application of Bicknell's analysis to 3C 66B must await multi-epoch VLBI imaging of the source.

Evidence supporting the relativistic beaming model for FRIs comes from the recent discovery using observations at a single frequency (Parma et al. 1993) of a statistical preference for the counterjet side of a sample of low-luminosity sources to be less polarized, and by implication more depolarized: this is interpreted as evidence that the counterjet side is further away from us and seen through a larger amount of galactic material. It would therefore be of interest if the counterjet side of 3C 66B were shown to be more depolarized than the jet side: unfortunately we lack good polarization data for the counterjet at low frequencies (Section 3.7) and while this in itself might be evidence for the effect, it is certainly not conclusive. It is interesting to note that a preferentially depolarized counterjet occurs in 3C31 (Strom et al. 1983), a source similar in luminosity and structure to 3C 66B.

The sheath-like structure in the polarization maps suggests that there are two distinct régimes in the jet. This can be explained by a modification of the relativistic beaming model which supposes that the core of the jet is relativistic and is surrounded by a more rapidly decelerating shear layer, perhaps slowing by entrainment of surrounding material. The parallel-field sheath observed in the jet and counterjet would correspond to the shear layer. The generally more edge-brightened and diffuse counterjet could be the emission from a slow outer sheath surrounding a core which is invisible or very faint due to beaming away from the observer; the jet side, as observed, would be expected to be centre-brightened at all times (unless its core velocity were very high indeed). The observed differences in the thicknesses of the parallel-field sheaths in the jet and counterjet would follow from the different beaming of the two cores.

4.2 Polarization

Laing (1993) uses a version of the core-sheath model described above to explain the change from parallel to perpendicular magnetic field direction often seen in FRI sources. In Laing's model the jet cores have a magnetic field with no longitudinal component and the shear layers have a longitudinal magnetic field. Close to the nucleus the bulk velocities of the cores of the counterjet and jet are highly relativistic: the emission from the cores is therefore very strongly beamed and invisible to an observer (if the source is at a significant angle to the line of sight) so that the $B_{\|}$ field from the shear layer dominates. As the jet decelerates the $B_{\perp}$ component in its centre becomes more important, so a changeover from parallel to perpendicular magnetic field direction is observed. In the case of 3C 66B, however, the model fails to explain the parallel polarization in the bright knots B and C: these are presumably features of the jet core and so in Laing's model should have a B-field perpendicular to the jet axis, while any region with parallel field structure should be edge-brightened if resolved. If we wish to retain a core-sheath model, we must assume that both the slow sheath and the fast core initially have longitudinal magnetic field, but that something happens early on to rotate the direction of the field in the core: on the jet side of 3C 66B this would occur near knot D (2.5 kpc from the nucleus), while in the counterjet we would have to suppose it to take place somewhere before the first good detection of perpendicularly-polarized flux, also at 2.5 kpc from the nucleus.

In general, the changeover in polarization configuration can be understood in terms of a magnetic field initially dominated by a longitudinal component which becomes less important as the jet expands. The magnetic field may be ordered (uniform or helical) or partially ordered (Laing 1981). Unfortunately, the presence of a longitudinal-field sheath makes it difficult to define the parameters of the region in which field turnover is occurring and therefore difficult to extract any information on the physics. We can say that in 3C 66B the change is not clearly related to any structure in total intensity, whereas for a model in which the jet is coming into equilibrium with its surroundings we should expect the change in orientation to be correlated with a drop in surface brightness (as in 3C219, for example; Clarke et al. 1992). The field continues to be longitudinal after the knot B, and it would appear that (as in 3C31; Fomalont et al. 1980) the expansion necessary to allow the transverse field to dominate must only be by a small factor.

4.3 Bending and wiggles

The smooth bending on kiloparsec scales of the jets in the maps we show here is suggestive of a motion of the source to the northwest, similar to those which are thought to bend the tails of narrow-angle tail radio galaxies (which are often, like 3C66B, outlying members of clusters). However, the large-scale lobe structure does not follow this curve, and includes some low-brightness regions which we would expect to be moving away from the nucleus at lower velocities (although they should also be denser) and so to be more affected by such a motion. A simple explanation of this sort is difficult to contrive.

Alternatively, the bending may just be the result of jet propagation into a non-symmetrical medium. The distorted isophotes of the host galaxy seen by Fraix-Burnet et al. (1989a) may be some evidence for this. 3C 66B is an interacting galaxy, with a companion to the SE of the radio source, but the mass of the companion is sufficiently low that orbital displacements are unlikely to have produced these large-scale variations in jet direction, and the orbital period is probably too long in any case (Balcells et al. 1995). It therefore does not seem possible to explain the large-scale structure of the source (i.e. the apparent sudden changes of direction of the outflow) without invoking a significantly clumpy environment. If the source axis is close to the line of sight then the bending is exaggerated by projection; LJP suggest that a model of this sort might explain a number of the peculiar features of the source on the large scale (see also section 4.1).

The small-scale (~ 1 kpc) wiggles in the jet ridge line, on the other hand, could be attributed to precession of the central collimator, to fluid flow instabilities or to gravitational effects from the companion galaxy. Precession seems physically unlikely: there is no obvious similar effect in the counterjet, and on the most conservative estimates of velocity the collimator would have to wobble through angles of several degrees on timescales of $\sim 10^5$ yr, which is several orders of magnitude less than the timescales for forced precession of a 10^8 M$_\odot$ black hole (Rees 1978). Orbital interaction with the companion suffers from the same problem of implausibly short timescales, leaving some sort of fluid flow instability as the best answer. If these wiggles are evidence for similar motions in the parts of the jet nearest the nucleus, a model in which the inner jet is relativistically beamed and the angle between the bulk velocity and the line of sight is changing slightly might explain some of the small-scale variations of brightness and magnetic-field direction in this area.

4.4 Small scale structure

The jet mapped at high resolution (Fig. 2) is roughly 3.5 arcsec across (at knot E): at this resolution and sensitivity we are probably only seeing the core of the jet, and not much of the parallel-field sheath. The jet is strongly centre-brightened. There is some evidence for a double-stranded filamentary structure in both the radio and the optical wavebands. Macchetto et al. (1991) suggest that this structure might be explained in terms of the helical-field models of Königl & Choudhuri (1985): here the filaments (according to JSMM) would be the boundaries of a twisted helical magnetic field tube and the banding across it would represent twists in the helix. Apart from the tentative nature of the evidence for filaments in the radio, one important objection to this model is provided by the magnetic field structure in our maps. If the field were as described by Königl & Choudhuri, we would expect to see changes (from parallel to perpendicular and back) in the direction of the magnetic field in the jet, strongly associated with the positions of bright knots. In fact the field is parallel initially, slightly oblique in knot B and then parallel to the jet again, turning to a wholly perpendicular configuration before the end of the proposed filamentary structure (shortly after knot D).

4.5 Spectral index and reacceleration

An important problem is raised by the radio-optical spectral index results of JSMM. They find that the spectral index is approximately constant ($\alpha = 0.8$ between 15 GHz and the optical) over a region 1 kpc across in the inner 5 kpc of the jet. When combined with our radio spectral index results, described above (section 3.6), this shows that the *spectrum* of the emitting particles is also approximately constant throughout this region; the spectral index is flat (0.5) in the radio and steep (1.4: JSMM) in the optical, so that the spectrum must be curved with a transition frequency somewhere between 15 and 10^6 GHz.

As JSMM point out, the synchrotron lifetime of the optically radiating electrons is short. If we define the lifetime t as the time taken for the synchrotron break frequency to become equal to the frequency of emission ν, then

$$t = \left(\frac{CB}{(B^2 + B_p^2)^2 \nu}\right)^{\frac{1}{2}} \tag{1}$$

(Leahy 1991) where B is the magnetic field strength, B_p is the equivalent magnetic field to the energy density in photons u_p ($B_p = \sqrt{2\mu_0 u_p}$; this term describes losses due to inverse-Compton scattering of background photons) and C is a constant which in useful units is 2.5×10^3 nT^3 Myr^2 GHz. The magnetic field strength B is not particularly well known. The only estimates come from minimum energy/equipartition arguments, but we cannot be certain that equipartition holds in this case. The estimates vary considerably depending on the part of the jet on which the calculation is done, and also depend on quantities such as the Hubble constant, the filling factor and the proton content of the jet about which we have little information. Further, the formula (1) holds for ageing in a constant B-field and photon energy density, and it is expected that both of these will change with distance from the nucleus; modelling the effect on particle energy distributions of this variation is difficult. The energy density in photons close to the nucleus will be dominated not by the cosmic background radiation but by starlight from the host galaxy (Owen, Hardee & Cornwell 1989: this should contribute an energy density of $\sim 10^{-12}$ J m^{-3} at 1 kpc, equivalent to $B_p = 1.6$ nT) and possibly by the continuum emission from the hidden AGN in 3C 66B.

With these caveats, some estimate can be made of the lifetimes of particles emitting in the optical. JSMM suggest an equipartition B-field of 10 nT; with $\nu = 10^6$ GHz (corresponding to the 3000-Å wavelength of the *HST* images) this gives a lifetime of 1.5×10^3 years. This field estimate is reasonable for the bright knots in the jet, through which (it is assumed) most of the electrons will have travelled; the equipartition field elsewhere in the inner jet is lower (3 – 4 nT, using a filling factor of unity, a cylindrical geometry for the jet, and assuming no energy in non-radiating particles) and so actual particle lifetimes may be higher. (It should be noted that either a lower filling factor, plausible given the suggestions of filamentary structure in the jet, or some contribution to the energy density from non-radiating particles would increase the equipartition B-field and so reduce the lifetimes. Highly relativistic bulk velocities make the observed surface brightness an overestimate of the emission in the bulk rest frame, and therefore reduce the inferred B-field, but the mildly relativistic velocities inferred from jet sidedness above should have little effect on the equipartition calculation.) The projected length of the optical jet is 5 kpc, so that the light travel time to the end of the optical jet is at least 1.5×10^4 yr. From the sidedness arguments above the bulk velocity of the electrons is unlikely to be greater than $0.5c$, and the deprojection factor is likely to be greater than 1.5; thus for some plausible jet parameters the most distant optically radiating particles have taken about 30 times their synchrotron lifetime to reach the end of the jet.

It can be seen from equation (1) that for a given B_p the maximum value of t is obtained when $B = B_p/\sqrt{3}$; thus without even knowing the magnetic field strength we can put limits on the lifetime from the energy density in photons. If $B = B_p/\sqrt{3} = 0.92$ nT, using the energy density given by Owen et al. (1989) for M87, then the maximum possible lifetime is 1.4×10^4 yr. This is still comparable to the light travel time to the end of the optical jet, and a factor of 3 or 4 shorter than a plausible electron travel time. For any other magnetic field strength the lifetime will be shorter. It would appear that we cannot retain a simple picture of acceleration in the nucleus while reproducing the observed constant spectrum unless the energy density in the photon background is less than $\sim 2 \times 10^{-13}$ J m^{-3}.

Possible alternative mechanisms include highly relativistic flow ($\gamma \sim 10$: $\beta > 0.995$), transport of the electrons in a 'low-loss channel' where the magnetic field (or at least the component perpendicular to the direction of bulk velocity) is much weaker than the equipartition value, and local reacceleration. Very high bulk velocities in the inner 5 kpc seem unlikely both in terms of acceleration mechanisms and because of the problems of deceleration referred to above, but they are not explicitly ruled out by the observations. JSMM remark that if a low-loss (or high bulk velocity) central channel were present we would expect to see steepening of the radio-optical spectrum away from the jet axis on comparatively small scales (even supposing diffusion at speeds close to c), which is not observed: 1500 yr corresponds to 500 pc, similar to the radius of the optical jet. Felten (1968), in the context of the optical jet in M87, points out that such a low magnetic-field channel might well be unstable (plasma instabilities would lead to particle scattering and possibly amplification of the magnetic field) on timescales shorter than the light-travel time to the end of the jet. Further, a low-loss channel would suffer losses to inverse-Compton scattering, as described above.

Similar conclusions have been reached for the two other well-studied optical jets in radio sources, M87 (e.g. Biretta & Meisenheimer 1993) and 3C273 (e.g. Röser & Meisenheimer 1991). The conclusions are slightly stronger in both, because the jets are brighter and narrower and the inferred equipartition B-fields stronger. In 3C273 inverse-Compton losses in the radiation field of the quasar definitely rule out the low-loss channel models.

If we adopt the hypothesis of local reacceleration in 3C 66B, we are left with the problem of where it is happening. One solution might be that the knots in the jet close to the nucleus are shocks at which first-order Fermi acceleration is taking place, as it is believed to do in the hotspots of classical double radio sources. However, the radio and radio-optical spectral indices of the knots are not distinguishable from those of the dimmer inter-knot material around them, which reduces the probability that they are privileged sites for particle acceleration. If acceleration took place only at the knots then there should be significant loss in the optical in the regions between them, again involving spatial scales of the order of 500 pc. However, the long mean free path lengths of the high-energy electrons (Meisenheimer et al. 1989) may 'smear out' the localization of the acceleration sites, and therefore make spectral variation less detectable.

In simple versions of the 'turbulent jet' model described above (section 4.1), particle acceleration occurs by a second-order Fermi process driven by turbulence throughout the jet. However, the shear this would produce is sufficient to maintain a magnetic field parallel to the jets at all times (Leahy 1991) and this is not observed; a consistently parallel field is only seen in the outer edges of the jet. It seems that the reacceleration cannot be confined to a boundary layer in 3C 66B if we are to identify the entraining region with the sheath observed in polarization, since the optical jet is well within it (there is no evidence for optical emission from the sheath regions with the sensitivity so far achieved). It may therefore be necessary to postulate *two* reacceleration processes; large-scale turbulent reacceleration in the outer regions of the jet, sufficient to account for the sub-adiabatic brightness decline of the jet on large scales, and some unknown process to drive the particle acceleration responsible for the optical jet. This process must also account for the constant and curved (rather than strictly power-law) spectrum along the jet, which is observed despite the large variations in surface brightness (and therefore inferred magnetic field).

In the Bicknell model the first bright knot B in 3C 66B would be identified with the site of the onset of turbulence, with the knots A being tracers of a much more efficient and free supersonic jet which undergoes a reconfinement shock at B when it comes into equilibrium with the pressure in the galactic atmosphere. Since the jet is still very one-sided after knot B, the relativistic beaming model requires that the post-shock velocity be relativistic, and at first sight it needs to be quite high to account for the brightness difference between knot B (which should be dominated by post-shock material) and its (unseen) counterpart in the counterjet. Bicknell (1994) claims that such brightness contrasts may be understood in terms of oblique relativistic shocks; the fact that the knot B appears to be aligned at an angle to the main jet axis may be some indication that this is correct. It should be possible to test whether the knot B is the standing shock commonly seen in hydrodynamical models of supersonic jets propagating into galactic atmospheres by searching for a proper motion; however, this would require very high-resolution multi-epoch observations. This has been done in M87 (Biretta, Zhou & Owen 1995) but would be much more difficult in 3C 66B because of its lower surface brightness and larger size scales. If knot B were moving at similar velocities to the brightest knot in M87 ($\sim 0.5c$, comparable to the velocity inferred from sidedness arguments for knot B) it would correspond to an angular motion of ~ 0.3 milliarcsec per year, nearly an order of magnitude smaller than the typical motions detected by Biretta et al.

4.6 Comparison with other sources

Table 3 shows the properties of some well-known jets in nearby FRI sources for comparison with those of 3C 66B. Unfortunately, the best-mapped sources are those least similar to 3C 66B. The jet in M87 has been mapped exhaustively, and the similarity of its optical counterpart to 3C 66B's has been discussed above; but M87 is in many ways more similar to a classical double source than it is to 3C 66B, and its jet is similar in opening angle (6°) and (as far as we can tell) in structure to those found in FRIIs or wide-angle tail sources. It has generally parallel magnetic fields (except at some bright knots) and is much shorter than the jets in 3C 66B. The model by Biretta (1993) suggests that the M87 jet is relativistic for much of its length and aligned at 40° to the line of sight: there is no observable counterjet, perhaps due to beaming effects. Biretta et al. (1995) claim to detect kpc-scale proper motion indicating $\gamma \sim 3$ in the inner jet. NGC6251 is another one-sided jet with initial parallel-field structure: its knotty inner structure and areas of oblique magnetic field are superficially similar to those in the jet side of 3C 66B, but this inner region extends over 75 kpc (an order of magnitude longer than in 3C 66B). The jet-counterjet flux ratio is $\sim 130 : 1$ over the first 250 arcsec from the nucleus, implying an angle to the line of sight of less than 45° on a naïve relativistic beaming model (using the spectral index of 0.64 in Perley et al. 1984). An *HST* image of NGC6251 (Crane 1993) shows no optical jet, however.

The jets in well-studied sources more similar to 3C 66B have generally been mapped at spatial resolutions insufficient to reveal detailed sub-kpc structure of the jet close to the nucleus, so it is not clear whether the filamentary and knotty structure we observe is common to all sources. The best available images of NGC315, 3C31, 3C296, IC4296 (PKS 1333–33) and 3C449 all show a perpendicular field structure beyond a few kpc from the nucleus, and with sufficient resolution the part of the jet closest to the nucleus shows a parallel field. The 'sheath' structure seen in 3C 66B is often lacking, but we have shown that high resolution and sensitivity are necessary for its detection (cf. the maps at 3-kpc resolution of 3C 66B in LJP, which show only a few traces of this structure). In 3C31 (Fomalont et al. 1980; Strom et al. 1983) and NGC315 (Willis et al. 1981) the central parallel field is only detected on the jet side. This is very like what we find in 3C 66B at low resolution, and is consistent with a beamed jet at a moderate angle to the line of sight: both sources have significant jet-counterjet asym-

Table 3. Parameters of some well-known jets in FRI sources

Name	z	Length (kpc)	Sides	Polarization structure Parallel up to:	Perpendicular from:	Res'n (kpc)	Reference
NGC315	0.0167	480	2	12 kpc on jet side	12 kpc on jet side: parallel sheath in counterjet	0.6	Venturi et al. (1993)
3C31	0.0167	28	2	5 kpc on jet side	5 kpc: parallel sheath	2.6	Burch (1977) Fomalont et al. (1980)
3C 66B	0.0215	90	2	3.75 kpc on jet side	3.75 kpc: parallel sheath	0.15	This paper
3C75(N)	0.0240	60	2	6 kpc on both sides	6 kpc	1.5	Owen et al. (1985) Our observations (unpublished)
3C75(S)	0.0240	60	2	?	12 kpc (or less)	1.5	Owen et al. (1985) Our observations (unpublished)
3C83.1B	0.0255	36	2	24 kpc	24 kpc: parallel sheath	0.6	O'Dea & Owen (1986)
M84	0.0029	6.6	2	?	300 pc (or less)	0.46	Laing & Bridle (1987)
M87	0.0041	3.6	1	Whole length, except at bright knots	N/A	0.012	Biretta (1993)
IC4296	0.0129	260	2	6 kpc on both sides	6 kpc (parallel at jet edges at bends)	1.2	Killeen, Bicknell & Ekers (1986)
3C296	0.0237	100	2	6 kpc on jet side	6 kpc	1.5	Leahy & Perley (1991) Our observations (unpublished)
NGC6251	0.024	320	1	60 kpc with regions of oblique field	60 kpc: parallel sheath	0.75	Perley, Bridle & Willis (1984)
3C449	0.0171	38	2	?	4.5 kpc (or less)	2.1	Perley, Willis & Scott (1979)

Jet

lengths are taken from Bridle & Perley (1984) modified to $H_0 = 50\ \mathrm{km\,s^{-1}\ Mpc^{-1}}$.

metry and show one-sided jets on small scales (Parma, Cameron & de Ruiter 1991: Venturi et al. 1993). High-resolution images of the jets in NGC315 are strikingly similar to our maps of 3C 66B, showing a narrow bright jet and a shorter and more diffuse counter-jet. Bicknell (1994) fits his model of a relativistic entraining jet to the parsec- and kiloparsec-scale features of NGC315 with success. In contrast IC4296, with two very symmetrical jets, has parallel magnetic fields in the inner 6 kpc of both. In the relativistic beaming model this would be interpreted as a source close to the plane of the sky. 3C83.1B (NGC1265) is a narrow-angle tail source with similar symmetry and polarization; it bends through a considerable angle before changing from a parallel to perpendicular field configuration. This is further evidence to suggest that the changeover is not directly connected with deceleration from a relativistic regime, if the shape of 3C83.1B is due to ram pressure as is usually suggested.

5 CONCLUSIONS

We have mapped the jets in 3C 66B in polarization and total intensity on scales ranging from 0.15 to 30 kpc. A model in which the jets are similar in power and consist of a relativistic central core surrounded by a slower outer sheath seems to fit the available data well, although significant deceleration on 10-kpc scales is necessary. In this model the jet is (at least initially) at an intermediate angle to the line of sight. Local reacceleration in the core of the jet is probably required to explain the radio and radio-optical spectral index. Polarization maps show a clearly delineated parallel-field sheath, explained as a shear layer at which the jets are interacting with the surrounding medium; the field in the core of the jet changes orientation from a parallel to a perpendicular configuration. There is evidence for this kind of behaviour in a number of other well-studied radio sources.

ACKNOWLEDGEMENTS. We thank Craig Mackay and an anonymous referee for helpful comments on an earlier draft of the manuscript. The NRAO Very Large Array is operated by Associated Universities Inc. under contract with the National Science Foundation; we are grateful to the director and staff of the VLA for their assistance. MJH acknowledges a studentship from the PPARC.

REFERENCES

Balcells M., Morganti R., Oosterloo T., Pérez-Fournon I., González-Serrano J.I., 1995, A&A, in press
Bicknell G.V., 1986, ApJ, 305, 109
Bicknell G.V., 1994, ApJ, 422, 542
Bicknell G.V., de Ruiter H.R., Fanti R., Morganti R., Parma P., 1990, ApJ, 354, 98
Biretta J.A., 1993, in Burgarella D., Livio M., O'Dea C., eds, Astrophysical Jets, Cambridge University Press, Cambridge, p. 263
Biretta J.A., Meisenheimer K., 1993, in Röser H.-J., Meisenheimer K., eds, Jets in Extragalactic Radio Sources, Springer-Verlag, Berlin, p. 45
Biretta J.A., Zhou F., Owen F.N., 1995, ApJ, in press
Bridle A.H., Perley R.A., 1984, ARA&A, 22, 319
Burch S.F., 1977, MNRAS, 181, 599
Burch S.F., 1979, MNRAS, 187, 187
Butcher H.R., van Breugel W., Miley G.K., 1980, ApJ, 235, 749
Clarke D.A., Bridle A.H., Burns J.O., Perley R.A., Norman M.L., 1992, ApJ, 385, 173
Crane P., 1993, in Röser H.-J., Meisenheimer K., eds, Jets in Extragalactic Radio Sources, Springer-Verlag, Berlin, p. 223
Felten J.E., 1968, ApJ, 151, 861
Fomalont E.B., Bridle A.H., Willis A.G., Perley R.A., 1980, ApJ, 237, 418
Fraix-Burnet D., Nieto J.-L., Lelièvre G., Macchetto F.D., Perryman M.A.C., di Serego Alighieri S., 1989a, ApJ, 336, 121
Fraix-Burnet D., Nieto J.-L., Poulain P, 1989b, A&A, 221, L1
Giovannini G., Venturi T., Feretti L., Comoretto G., Wehrle A.E., 1993, in Röser H.-J., Meisenheimer K., eds, Jets in Extragalactic Radio Sources, Springer-Verlag, Berlin, p. 65
Jackson N., Sparks W.B., Miley G.K., Macchetto F., 1993, A&A, 269, 128
Killeen N.E.B., Bicknell G.V., Ekers R.D., 1986, ApJ, 302, 306
Komissarov S.S., 1993, in Röser H.-J., Meisenheimer K., eds, Jets in Extragalactic Radio Sources, Springer-Verlag, Berlin, p. 45

Königl A., Choudhuri A.R., 1985, ApJ, 289, 173
Laing R.A., 1981, ApJ, 248, 87
Laing R.A., 1993, in Burgarella D., Livio M., O'Dea C., eds, Astrophysical Jets, Cambridge University Press, Cambridge, p. 95
Laing R.A., Bridle A.H., 1987, MNRAS, 228, 557
Leahy J.P., 1991, in Hughes P., ed., Beams and Jets in Astrophysics, Cambridge University Press, Cambridge, p. 100
Leahy J.P., Perley R.A., 1991, AJ, 102, 537
Leahy J.P., Jägers W.J., Pooley G.G., 1986, A&A, 156, 234
Maccagni D., Tarenghi M., 1981, ApJ, 243, 42
Macchetto F., Albrecht R., Barbieri C., 1991, ApJ, 373, L55
Matthews T.A., Morgan W.W., Schmidt M., 1964, ApJ, 140, 35
Meisenheimer K., Röser H.-J., Hiltner P.R., Yates M.G., Longair M.S., Chini R., Perley R.A., 1989, A&A, 219, 63
Northover K.J.E., 1973, MNRAS, 165, 369
O'Dea C.P., Owen F.N., 1986, AJ, 301, 841
Owen F.N., O'Dea C.P., Inoue M., Eilek J.A., 1985, ApJ, 294, L85
Owen F.N., Hardee P.E., Cornwell T.J., 1989, ApJ, 340, 698
Parma P., Cameron R.A., de Ruiter H.R., 1991, AJ, 102, 1960
Parma P., Morganti R., Capetti A., Fanti R., de Ruiter H.R., 1993, A&A, 267, 31
Perley R.A., Willis A.G., Scott J.S., 1979, Nat, 281, 437
Perley R.A., Bridle A.H., Willis A.G., 1984, ApJS, 54, 291
Rees M.J., 1978, Nat, 275, 516
Röser H.-J., Meisenheimer K., 1991, A&A, 252, 458
Strom R.G., Fanti R., Parma P., Ekers R.D., 1983, A&A, 122, 305
Venturi T., Giovannini G., Feretti L., Comoretto G., Wehrle A.E., 1993, ApJ, 408, 81
Willis A.G., Strom R.G., Bridle A.H., Fomalont E.B., 1981, A&A, 95, 250